Kinetics of Micelle Formation with Change of Micelle Shape in a Dilute Solution of Diblock Copolymers

Kayori Iyama and Takuhei Nose*

Department of Polymer Chemistry, Tokyo Institute of Technology, 2-12-1 Ookayama, Meguro-ku, Tokyo 152-8552, Japan

Received March 31, 1998; Revised Manuscript Received August 18, 1998

ABSTRACT: By means of time-resolved static and dynamic light scattering, association processes of micelles are investigated for polystyrene-*block*-poly(dimethylsiloxane) in the mixed selective solvent, *n*-octane/methylcyclohexane, where the micelle can take either a hollow spherical structure or a hollow cylindrical structure, depending on the condition of micelle formation. The following are revealed: The cylindrical micelles are not thermodynamically stable ones but are temporally formed in the course of micelle formation. Micellization from the unimer state or micellar relaxation from one micelle state to another micelle state does not monotonically proceed to reach the destination but passes through the formation of cylindrical micelles having association numbers larger than those of both initial and equilibrium micelles. At lower temperatures and lower concentrations, the cylindrical micelles with larger size and longer time stability are easily formed. The formation of the large cylindrical micelles is the result of a rapid growth of micelles by elongating into the cylindrical shape, which may come from bilayer structure of the micelles.

Introduction

Various association behaviors of block copolymers in selective solvents have attracted a great deal of attention from both theoretical and experimental viewpoints.[1] Some investigations[2−5] have revealed that changes of temperature and/or concentration induce changes of micelle shapes, for example, from spherical to cylindrical ones. Such changes have commonly been observed in conventional low molecular weight surfactant micelles as well.[6] Block copolymer micelles, however, often show more complex association behavior[7−16] than the conventional surfactant micelles. For instance, in the dilute solution of polystyrene-*block*-polybutadienes studied by Tsunashima,[7] *larger* micelles appear at *lower* concentrations, in contrast to the usual finding that larger micelles are formed at higher concentrations. Price et al.[8] and Stejskal et al.[9−11] have found that some block copolymer micelles formed on heating in solution were different from those on cooling. Eisenberg et al.[12,13] have revealed morphological complexity of diblock copolymer aggregates in solution depending on the composition of mixed solvent and the preparation procedures of solution. These experimental results suggest that observed micelles in polymeric systems are not always equilibrium ones but appear as nonequilibrium ones during the micellization and/or relaxation processes of micelles. In fact, our previous study[16] on micellar solutions of polystyrene-*block*-poly(dimethylsiloxane) (PS-*block*-PDMS) has more directly demonstrated that micelle size and shape have the process dependency. That is, the structural rearrangements between spherical and cylindrical micelles are only observed during the heating process, but no appreciable changes of micelle size and shape are observed during the cooling processes. Thus, the kinetic aspect is indispensable for understanding the observable size and shape of micelles. Almost none of studies have been reported on the relationship between micellar structures and micellization kinetics. The purpose of this paper is to manifest the importance of micellization kinetics in explaining the structure of actually observed micelles and to demonstrate that the structural changes can be induced by completely kinetic factors.

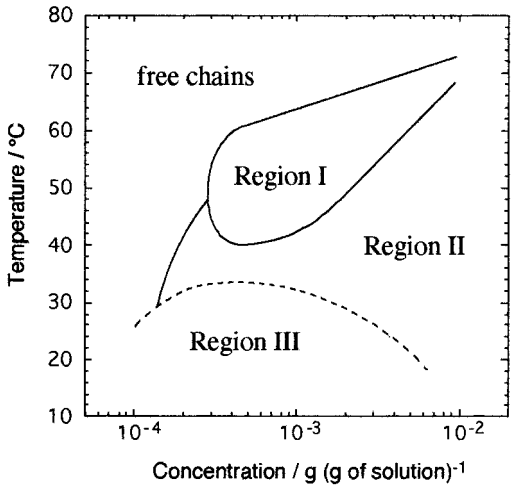

Figure 1. Temperature−concentration diagram of PS-*block*-PDMS in C_8/MCH obtained on heating from 12 to 72 °C at the rate of 3 °C h^{-1}. Three distinct regions appear in addition to the unimer region.[16]

In the previously studied micellar solution of PS-*block*-PDMS in a selective solvent, three different regions appear *on heating* after quenching from the unimer state, as illustrated in Figure 1. Region I is the so-called anomalous-micellization region. In region II, stable vesicles with the association number of about 10^3 are formed. Region III at *lower* concentrations is the region of the large hollow cylindrical micelles, to which we will here pay attention since it does not appear on cooling from the unimer state, as shown in Figure 2. The difference in formed micellar structure between heating and cooling processes must come from the thermal history of the solution in the course of micellization from the unimer state and/or micellar rearrangements in cooling processes. This process dependency suggests that region III may not be an equilibrium phase, but may appear kinetically.

10.1021/ma980501t CCC: $15.00
Published on Web 09/26/1998

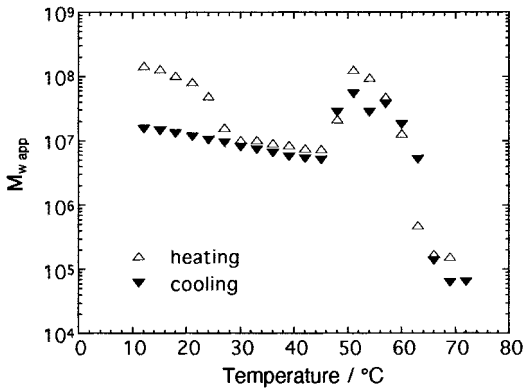

Figure 2. $M_{w,app}$ against temperature on heating (△) from 12 °C and on cooling (▼) from 72 °C at the concentration $C = 1.90 \times 10^{-3}$ g (g of solution)$^{-1}$.

In this study, by static and dynamic light scattering, we investigate kinetics of micelle formation in region III to demonstrate that the region really kinetically appears and reveal details of the time evolution of association number and shape of micelles formed in this region. That is, weight-average molecular weights, radii of gyration and hydrodynamic radii of micelles are measured as a function of *time* for two types of conditions: (1) micellar rearrangements, i.e., the relaxation of micelles from one micelle state to another micelle state, and (2) micellization from the unimer state. In the following sections, we first describe experimental methods, followed by presenting obtained data for the kinetics of the micelle formation, and in the subsequent section we evaluate the structural change of micelles with the increase of association number. Finally, we discuss the mechanism of micellization processes accompanied with structural rearrangements in the last section.

Experimental Section

Materials. Number-average molecular weights of PS and PDMS blocks are 7.8×10^3 and 3.2×10^3, respectively. The molecular-weight distribution index M_w/M_n of PS-*block*-PDMS is 1.18. The solvent is a mixture of *n*-octane (C_8) and methylcyclohexane (MCH) with the composition of C_8/MCH = 1.23 by weight. The solvent is isorefractive and selective for PDMS. Details of the materials have been described in the previous paper.[16]

Light Scattering Measurements. The light scattering apparatus was a laboratory-made one[16] equipped with an Ar-ion laser operating at a wavelength $\lambda = 488$ nm as the light source and an ALV/SO-SIPD single photon detector as the detector. In time-resolved static light scattering at experimental times shorter than 1800 s, integrated scattered-light intensities at scattering angles of 60° and 120° were simultaneously measured through a dual-angle optical system. At times longer than 1800 s, the intensity was measured at every 3° by scanning the scattering angle θ from 30° to 120°. It took about 900 s to obtain one set of data as a function of θ. In the time-resolved dynamic light scattering, the autocorrelation function of scattered-light intensity was measured mostly at $\theta = 30°$ with an ALV-5000 digital multiple-τ correlator. The accumulation time was 20 and 600 s at shorter and longer experimental times, respectively.

Excess Rayleigh ratio $\Delta R(\theta)$ was calculated from the measured excess scattered-light intensity using the intensity of benzene as standard with the Rayleigh ratio of benzene given in the literature.[17−19] The conventional analysis for determination of weight-average molecular weight and radius of gyration could not be applied to the present time-resolved measurement, so that apparent weight-average molecular weight $M_{w,app}$ and apparent radius of gyration $R_{g,app}$ were evaluated without extrapolation to the dilute limit. $M_{w,app}$ and $R_{g,app}$ are defined as follows.

$$M_{w,app} = \frac{\Delta R(0)}{KC} \tag{1}$$

$$R_{g,app}{}^2 = \frac{3\lambda^2 M_{w,app}(\text{initial slope})}{16\pi^2 n^2} \tag{2}$$

K is the optical constant defined by $K = 4\pi^2 n^2 (\partial n/\partial C)^2/(N_A \lambda^4)$, where n, λ, and N_A are the refractive index of the solvent, the wavelength of incident beam, and the Avogadro constant, respectively. The refractive-index increment $\partial n/\partial C$ was measured by a differential refractometer (Union Giken RM-102). $KC/\Delta R(0)$ and (initial slope) are the intercept and the initial slope in the plots of $KC/\Delta R(0)$ vs $\sin^2(\theta/2)$ at finite concentrations, respectively. Since the refractive index of the solvent is almost equal to that of PDMS, the obtained $R_{g,app}$ can be regarded as that of PS parts of a micelle.

The electric-field time correlation function obtained by dynamic light scattering was analyzed by the cumulant method of the second order to evaluate the average decay rate $\bar{\Gamma}$ and the variance $\mu_2/\bar{\Gamma}^2$. The diffusion coefficient D was calculated by $\bar{\Gamma} = Dq^2$, where q is defined as $q = (4\pi n/\lambda)\sin(\theta/2)$. The condition of $R_{g,app}q \geq 1$ was satisfied in most of the cases, except for a few cases where $R_{g,app}$ was extremely large. Similarly to $M_{w,app}$ and $R_{g,app}$, the extrapolation of D to zero concentration was not applicable, so that apparent diffusion coefficient D_{app} at a finite concentration without the extrapolation was regarded as that at the dilute limit. From the D_{app}, apparent hydrodynamic radius $R_{h,app}$ was calculated by the equation

$$R_{h,app} = \frac{k_B T}{6\pi\eta D_{app}} \tag{3}$$

where k_B, T, and η are the Boltzmann constant, absolute temperature, and solvent viscosity, respectively. The solvent viscosity was measured by a Ubbelohde-type viscometer as a function of temperature.

A stock solution with the concentration of 1×10^{-2} g (g of solution)$^{-1}$ was prepared by dissolving the block copolymer in the mixed solvent and was kept at 85 °C for 1 h and at room temperature for 1 day with mild stirring. The stock solution was filtered through a Millipore filter of nominal pore size of 0.5 μm into a dust-free optical tube at room temperature and diluted with the solvent filtered through a Millipore filter of nominal pore size of 0.2 μm to be of the desired concentration. The optical glassy tubes were flame-sealed under mild vacuum.

Before starting every experimental run, the solution was kept at 85 °C for 2 h to be completely decomposed into unimers. The time-resolved light scattering measurements were performed for different concentrations ranging from 1.38×10^{-3} to 3.72×10^{-3} g (g of solution)$^{-1}$ under the following two types of condition: (1) time evolution on cooling from 36 to 12 °C and subsequent time evolution at the constant temperature of 12 °C after the cooling and (2) time evolution at constant temperatures in region III after quenching from the unimer state. In the case of condition 1, the solution was first quenched from 85 to 36 °C and left at 36 °C in region II for 2 h so as to form equilibrium spherical micelles. $M_{w,app}$, $R_{g,app}$, and $R_{h,app}$ of spherical micelles at 36 °C become constant within 2 h, as shown in Figure 3, and the standing time at 36 °C does not influence the properties of micelles at 12 °C. Then, the solution was cooled to 12 °C in region III at different cooling rates. In condition 2, the solution was directly quenched from 85 °C down to several designated temperatures below the critical micellization temperature. The quenching of a sample solution was carried out by transferring the optical tube (diameter: 10 mm) containing the sample solution of about 2 mL from a thermostat for preheating at 85 °C into the light scattering apparatus controlled at an experimental temperature. The temperature was stabilized within 100 s after transfer of the sample tube and controlled within ±0.01 °C.

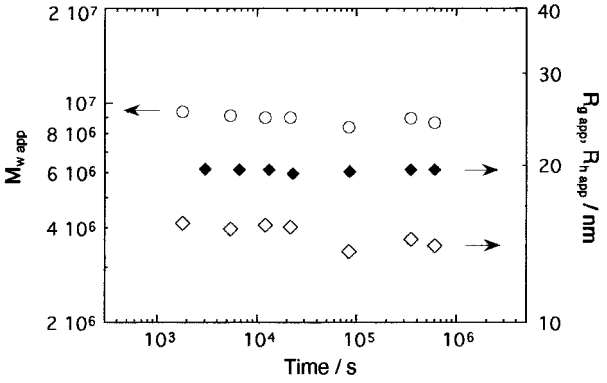

Figure 3. Changes of $M_{w,app}$ (○), $R_{g,app}$ (◇), and $R_{h,app}$ (◆) at 36 °C with the lapse of time after quenching from 85 °C at the concentration $C = 1.90 \times 10^{-3}$ g (g of solution)$^{-1}$.

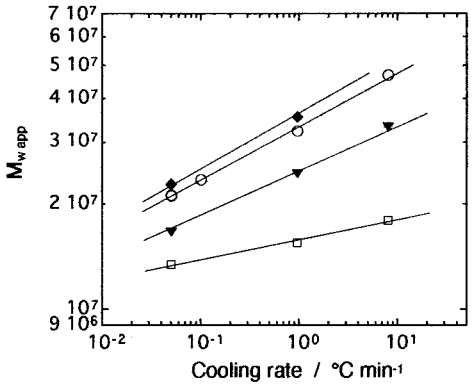

Figure 4. Cooling rate dependence of $M_{w,app}$ of micelles at 12 °C formed by cooling from 36 °C. The concentrations are 1.38×10^{-3} g (g of solution)$^{-1}$ (◆), 1.48×10^{-3} g (g of solution)$^{-1}$ (○), 1.90×10^{-3} g (g of solution)$^{-1}$ (▼), and 3.72×10^{-3} g (g of solution)$^{-1}$ (□). The plots are the data taken at the time when the temperature just reaches 12 °C. The lines are guides for the eye.

Results and Discussion

Micellar Rearrangements. Condition 1. Figure 4 shows the cooling rate dependence of the $M_{w,app}$ of micelles at 12 °C formed on cooling from 36 °C for various concentrations. It should be noted that the $M_{w,app}$ of initial micelles formed at 36 °C is almost independent of concentration, being around $M_{w,app} = 1.0 \times 10^7$. In contrast to this, the micelle formed at the *higher* cooling rate or at the *lower* concentration has the *higher* $M_{w,app}$. These dependences on cooling rate and concentration seem unlikely from the view of the common understanding that slower cooling and/or higher concentration away from the critical micellization concentration bring about larger micelles. This suggests that these micelles formed on cooling are not equilibrium ones.

Figures 5 and 6 represent the changes of $M_{w,app}$, $R_{g,app}$, and $R_{h,app}$ at 12 °C with the lapse of time after the cooling, along with those of the $M_{w,app}$ during the cooling from 36 to 12 °C. Arrows in Figure 5 indicate the time when the temperature reaches 12 °C. The $M_{w,app}$ is still increasing at 12 °C with the lapse of time and the increment of $M_{w,app}$ at 12 °C is *larger* at *higher* cooling rates (Figure 5a) or at *lower* concentrations (Figure 5b), except the highest cooling rate solution having higher values of $M_{w,app}$ from the beginning. The $R_{g,app}$ and $R_{h,app}$ also increase with the lapse of time, in parallel with the change of $M_{w,app}$ (Figure 6). A quantitative analysis of structural changes will be made by using these data in the later section.

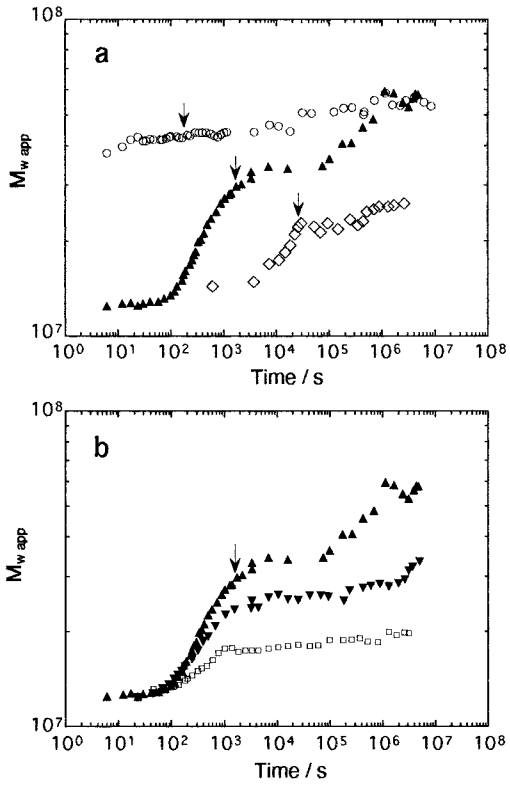

Figure 5. Time evolution of $M_{w,app}$ at 12 °C in condition 1. (a) Cooling rate dependence of $M_{w,app}$ at the concentration $C = 1.48 \times 10^{-3}$ g (g of solution)$^{-1}$. The cooling rates are 8.0 °C min^{-1} (○), 0.96 °C min^{-1} (▲), and 0.050 °C min^{-1} (◇). (b) Concentration dependence of $M_{w,app}$ at the cooling rate of 0.96 °C min^{-1}. The concentrations are 1.48×10^{-3} g (g of solution)$^{-1}$ (▲), 1.90×10^{-3} g (g of solution)$^{-1}$ (▼), and 3.72×10^{-3} g (g of solution)$^{-1}$ (□). Arrows indicate the time when the temperature reaches 12 °C.

The micelles formed at different cooling rates are not the same even at longer times over 10^6 s, as seen in Figures 5 and 6, which obviously shows that these micelles have not reached equilibrium and are still in the course of micellar rearrangements. The continuous increases in $M_{w,app}$, $R_{g,app}$, and $R_{h,app}$ seem to suggest that the equilibrium micelle is the larger one. However, it may not be true actually, because it is inconsistent with the observation that the *larger* micelles are formed at the *higher* cooling rates, as shown in Figure 4. The *lower* cooling rate should correspond to the *longer* time spent to form micelles and it is always true that the micelles approach the equilibrium at sufficiently *longer* times. This leads to the suggestion that the large micelle itself may be a nonequilibrium one, which is directly demonstrated by experimental observations in condition 2 of micellization from the unimer state.

Micellization from the Unimer State. Condition 2. Figures 7a and 8 show the time evolution of $M_{w,app}$, $R_{g,app}$, and $R_{h,app}$ of a micellar solution quenched from the unimer state as a function of temperature. The results clearly indicate nonmonotonical changes of the micelle size in the micellization from the unimer state. At an earlier stage of micellization, $M_{w,app}$ rapidly increases for a few minutes and reaches a maximum value, and then it slowly decreases with the lapse of time, approaching the value of the equilibrium micelles. $R_{g,app}$ and $R_{h,app}$ exhibit parallel changes with the change of $M_{w,app}$. Some previous investigations have demonstrated nonmonotonical changes of micelle size with

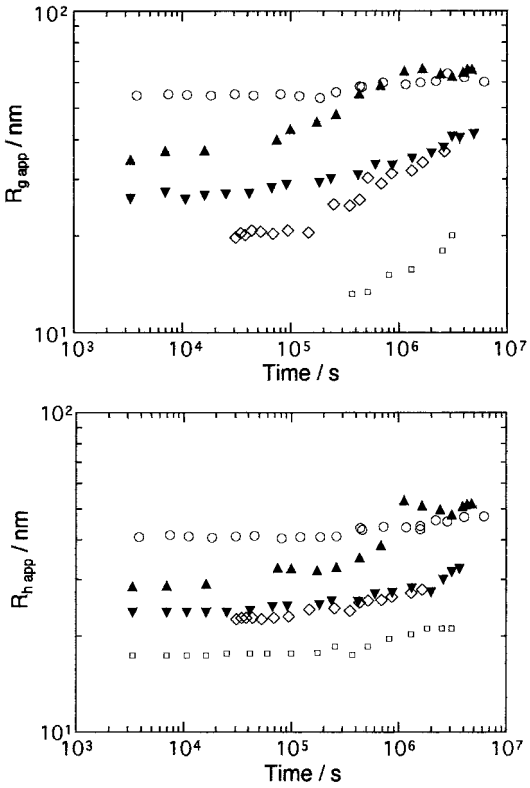

Figure 6. Time evolution of $R_{g,app}$ and $R_{h,app}$ at 12 °C in condition 1. The plots are for the solution of $C = 1.48 \times 10^{-3}$ g (g of solution)$^{-1}$ at the cooling rates of 8.0 °C min^{-1} (○), 0.96 °C min^{-1} (▲), and 0.050 °C min^{-1} (◇), and for the cooling rate of 0.96 °C min^{-1} at the concentrations of 1.90×10^{-3} g (g of solution)$^{-1}$ (▼) and 3.72×10^{-3} g (g of solution)$^{-1}$ (□).

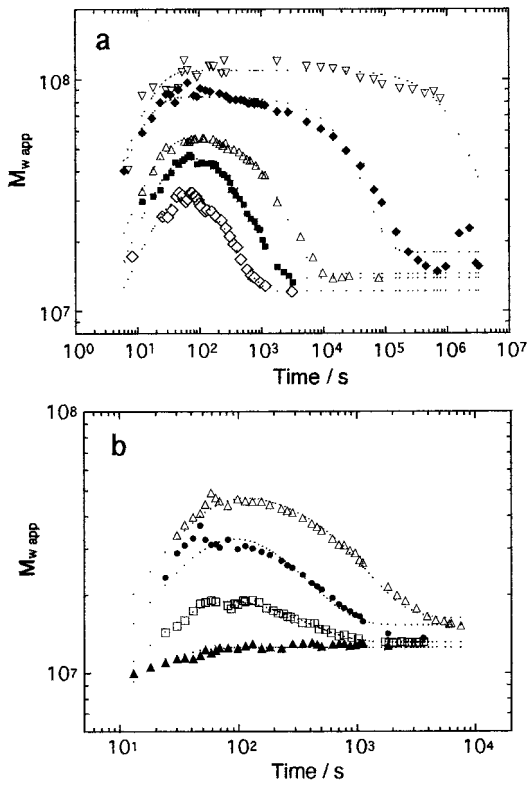

Figure 7. Time evolution of $M_{w,app}$ in condition 2. (a) Temperature dependence of $M_{w,app}$ at the concentration $C = 1.38 \times 10^{-3}$ g (g of solution)$^{-1}$. The temperatures are 12 °C (▽), 21 °C (◆), 27 °C (△), 30 °C (■), and 33 °C (◇). (b) Concentration dependence of $M_{w,app}$ at 27 °C. The concentrations are 1.38×10^{-3} g (g of solution)$^{-1}$ (△), 1.90×10^{-3} g (g of solution)$^{-1}$ (●), 2.51×10^{-3} g (g of solution)$^{-1}$ (□), and 3.72×10^{-3} g (g of solution)$^{-1}$ (▲). Dotted lines are the fitting curves obtained by using eq 4.

time during micelle formation.[20−22] Honda et al.[20] found the two processes of decomposition and recovery of micelles exhibiting the minimum of micelle size in micellar relaxation. Michels et al.[21] and Goldmints et al.[22] observed a rapid and large increase of scattered-light intensity followed by a rather slow and small decrease in micellization from the unimer state.

The maximum value of $M_{w,app}$ becomes *higher* with *decreasing* temperature. In other words, the micelle grows more rapidly and reaches the larger size by the first fast process at the lower temperature. Taking into account that the experimental cooling rate in condition 1 corresponds to the time scale of the fast process in condition 2, one can see that the temperature dependence of the micelle growth is equivalent to the cooling rate dependence of micelle size in condition 1. The slow process of decreasing micelle size becomes slower as the temperature decreases, so that once large micelles are formed by the fast process, they do not easily decompose to smaller ones at lower temperatures. At 12 °C, for example, the micelle size is kept almost constant for 1 week, although it decreases by a few 10%.

The concentration dependence of the time evolution of $M_{w,app}$ is shown in Figure 7b. The maximum value of $M_{w,app}$ *decreases* with the *increase* of concentration, and at $C = 3.72 \times 10^{-3}$ g (g of solution)$^{-1}$ the $M_{w,app}$ monotonically increases with time, showing no maximum. This concentration dependence is again consistent with the concentration dependence of micelle size observed in condition 1 shown in Figures 4 and 5b. Consequently, the consistencies in the micelle size and in both of the temperature and concentration dependences between conditions 1 and 2 indicate that the micelles formed near the maximum intensities in condition 2 correspond to those observed at longer times in condition 1 (Figure 5).

The time evolution of the polydispersity index $\mu_2/\bar{\Gamma}^2$ illustrated in Figure 9 also supports that the large micelles are nonequilibrium ones formed in the course of micellization. The values of $\mu_2/\bar{\Gamma}^2$ in condition 1 (Figure 9a) are around 0.1 and increase with the lapse of time at lower cooling rates, while those in condition 2 (Figure 9b) decrease with time in the slow process. These findings exactly correspond to proceeding and ending of the micellization, since larger values of $\mu_2/\bar{\Gamma}^2$ may indicate more deviation from the equilibrium, as is often the case in micellization processes.[23]

In conclusion, the above observations in the time evolution of micellar solutions under the two conditions clearly demonstrate that region III of the large cylindrical micelles does not indicate the presence of an equilibrium phase but appears because of kinetically formed associates.

To evaluate representative time constants of the fast and the slow processes in micellization from the unimer state, the time evolution of $M_{w,app}$ is approximated by the following function with respective single relaxation times for the fast and slow processes.

$$M_{w,app} = M_{w1}\{1 - \exp(-t/\tau_1)\} - (M_{w1} - M_{w2})\{1 - \exp(-t/\tau_2)\} \qquad (\tau_1 < \tau_2) \quad (4)$$

Constants M_{w1} and M_{w2} correspond to the increment of

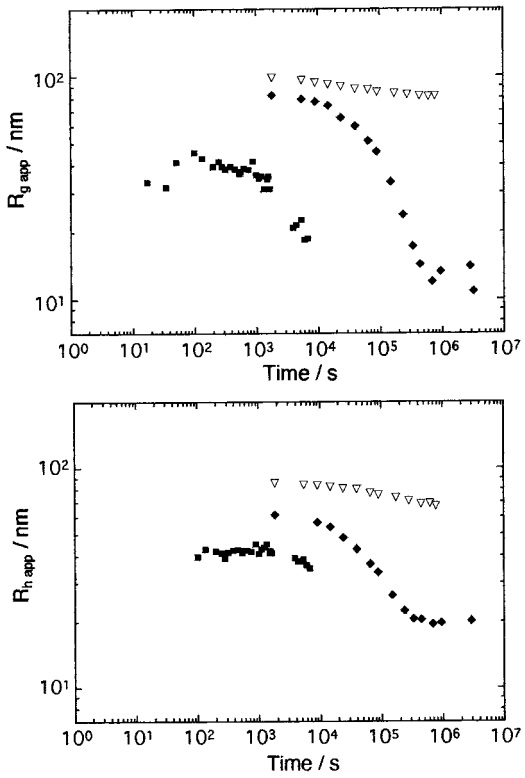

Figure 8. Time evolution of $R_{g,app}$ and $R_{h,app}$ in condition 2. The plots are for the solution of $C = 1.38 \times 10^{-3}$ g (g of solution)$^{-1}$ quenched from the unimer region to the different temperatures, 12 °C (▽), 21 °C (◆), and 30 °C (■). The data of 30 °C were taken in an experimental run different from that of $M_{w,app}$ shown in Figure 7, so that they do not exactly correspond to each other.

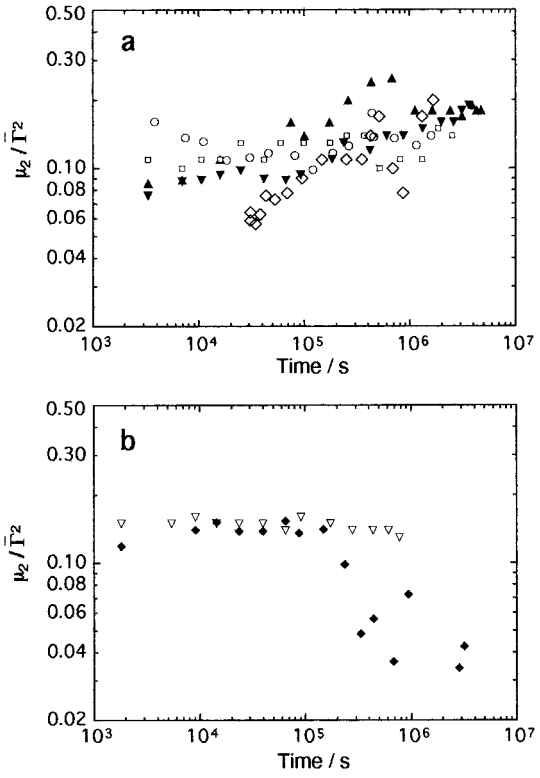

Figure 9. Time evolution of $\mu_2/\bar{\Gamma}^2$ in conditions 1 and 2. (a) Condition 1: The plots are for the solution of $C = 1.48 \times 10^{-3}$ g (g of solution)$^{-1}$ at the cooling rates of 8.0 °C min^{-1} (○), 0.96 °C min^{-1} (▲), and 0.050 °C min^{-1} (◇) and for the cooling rate of 0.96 °C min^{-1} at the concentrations of 1.90×10^{-3} g (g of solution)$^{-1}$ (▼) and 3.72×10^{-3} g (g of solution)$^{-1}$ (□). (b) Condition 2: The plots are for the solution of $C = 1.38 \times 10^{-3}$ g (g of solution)$^{-1}$ quenched from the unimer region to the different temperatures, 12 °C (▽) and 21 °C (◆).

the $M_{w,app}$ by the fast process and the $M_{w,app}$ at the equilibrium, respectively, neglecting the scattered-light intensity at the unimer state. Time constants τ_1 for the fast process and τ_2 for the slow process were obtained by the least-squares fitting of eq 4. Fitting curves are shown in Figure 7, and temperature and concentration dependences of the obtained parameters are plotted in Figure 10. In all cases, the time constant τ_1 is of the order of 10 s and almost independent of temperature and concentration. The concentration dependence of τ_2 is also weak, while the temperature dependence of τ_2 is so large that τ_2 at 21 °C is larger than τ_2 at 33 °C by about 100 times. The estimated τ_2 at 12 °C, for example, is around 1×10^6 s (≈2 weeks), so that the large micelle looks stable and is practically regarded as in a metastable state at lower temperatures. $M_{w,app}$ of the large micelle, M_{w1}, is about 10 times the equilibrium one (M_{w2}) at lower concentrations. The equilibrium micelle with $M_{w,app} \cong M_{w2}$ is not so large, changing its size with temperature and concentration very gradually. The M_{w2} as a function of temperature (Figure 10a) is comparable with the $M_{w,app}$ on the slow cooling shown in Figure 2. Namely, the micelles formed by the slower cooling seem to be close to the equilibrium ones. However, it should be pointed out that those formed on the slow cooling are not real equilibrium ones, but still changing with time, as shown in Figures 5a and 6.

Structural Changes in Conditions 1 and 2. In Figure 11, are shown log−log plots of $R_{g,app}$, $R_{h,app}$, and $R_{g,app}/R_{h,app}$ against $M_{w,app}$ in the both conditions 1 and 2. These three plots respectively make almost single master curves, showing that the micelle shape is approximately determined by the association number irrespective of micelle-formation conditions. The plots of log $R_{g,app}$ and log $R_{h,app}$ against log $M_{w,app}$ have considerably large slopes more than the value, 0.5, of a hollow sphere with a thin shell. This suggests that the shape of micelles changes probably into an elongated one with increasing association number. In fact, the ratio of $R_{g,app}/R_{h,app}$ changes from less than unity to more than unity with increasing $M_{w,app}$, clearly showing that the micelle shape changes from a spherical to cylindrical one with an increase of the association number, although $R_{g,app}$ measures the core part only while $R_{h,app}$ measures the whole of a micelle. In Figure 12 is shown further evidence for the elongation of micelles. That is, the ratio of D_{app} at 90° to D_{app} at 30° ($D_{app}(90°)/D_{app}(30°)$) becomes more than unity with the increase of $M_{w,app}$, which indicates a change to the nonspherical shape of micelles.

To show the micelle elongation with the increase of association number more quantitatively, we make an analysis of the micelle shape by using the model of a hemispherical hollow cylinder. Details of the analysis are described in the Appendix. The evaluated values of the total length of cylinder L_t including the hemisphere parts, the outside radius of the core part r_0, and the axis ratio $(L + 2r_0)/2r_0$ are shown in Figure 13. L_t keeps increasing with increasing $M_{w,app}$ over the whole range of $M_{w,app}$. r_0, at first, decreases and the axis ratio $(L + 2r_0)/2r_0$ increases relatively quickly at lower $M_{w,app}$'s, and then, with a further increase of $M_{w,app}$, r_0 increases and the axis ratio levels off. This change of the axis ratio is consistent with the change of $R_{g,app}/$

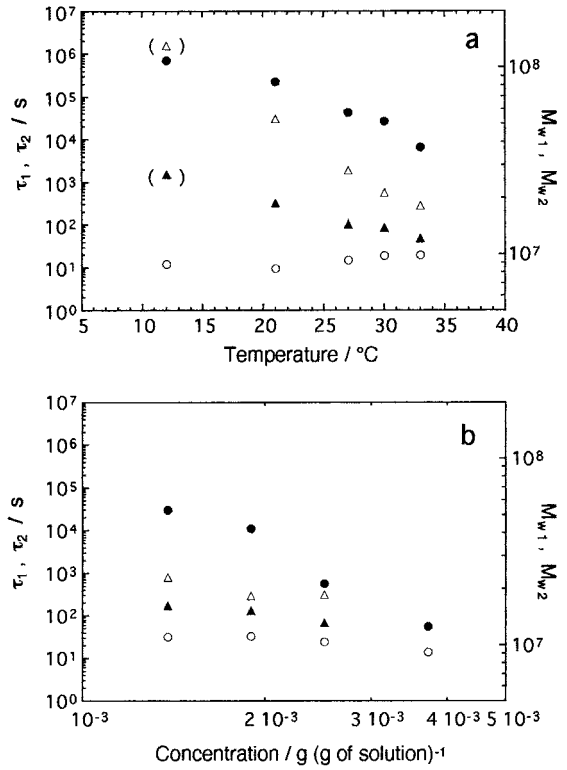

Figure 10. Plots of τ_1 (○), τ_2 (△), M_{w1} (●), and M_{w2} (▲) against the temperature (a) and the concentration (b) for condition 2. The data plotted in "parentheses" for τ_2 and M_{w2} at 12 °C were estimated in the following way because of the limited experimental time range: We first estimated the value of M_{w2} at 12 °C by the extrapolation of the data at 21−33 °C and fitted the experimental results of $M_{w,app}$ vs time to eq 4 with this value of M_{w2} to estimate the τ_2.

$R_{h,app}$ with $M_{w,app}$ shown in Figure 11. As the association number increases, the structure changes from the sphere to the elongated one with a little thinning of the diameter, and a further increase of association number is achieved by increasing both the length and the radius of the cylinder by keeping the axis ratio almost constant.

Mechanisms for Micellization Processes. In Aniansson−Wall (A−W) theory,[24−26] which assumes no occurrences of fusion and/or fission of micelles, the insertion and expulsion of unimers in to and out of micelles are only elemental processes in micellar relaxation kinetics. This leads to the presence of two distinguished processes, the fast and the slow processes: The fast process is accompanied by a change in the number of unimers under a constant number of micelles, and the following slow process involves a change of the total number of micelles with almost no change of the unimer number. The change of micelle number implies birth or extinction of micelles, which takes a long time under the condition of no excess free unimers. Such a kinetics for micelle formation and relaxation by the unimer insertion and/or expulsion is called the A−W mechanism. The A−W mechanism is basically applicable to diblock copolymer micelles in dilute solution, as demonstrated theoretically[27−29] and experimentally,[20,23,30−33] and by computer simulations.[34−36] The present micellization kinetics may be explained on the basis of the A−W mechanism as well.

In the micellization from the unimer state, the fast process is considered to correspond to the rapid formation of micelles with consumption of the excess unimers in the pool of solution, while in the slow process of the micellar solution approaching the equilibrium state, the micellar rearrangement proceeds with the gradual change in association number and the number of mi-

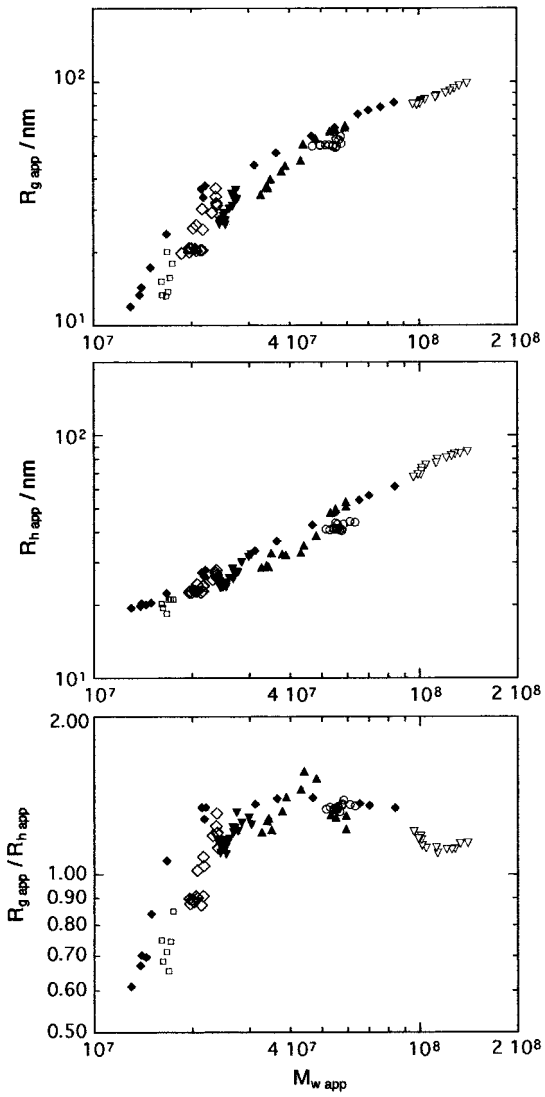

Figure 11. Relationships of $R_{g,app}$, $R_{h,app}$, and $R_{g,app}/R_{h,app}$ to $M_{w,app}$. For condition 1, the plots are for the solution of $C = 1.48 \times 10^{-3}$ g (g of solution)$^{-1}$ at the cooling rates of 8.0 °C min^{-1} (○), 0.96 °C min^{-1} (▲), and 0.050 °C min^{-1} (◇) and for the cooling rate of 0.96 °C min^{-1} at the concentrations of 1.90×10^{-3} g (g of solution)$^{-1}$ (▼) and 3.72×10^{-3} g (g of solution)$^{-1}$ (□). For condition 2, the plots are for the solution of $C = 1.38 \times 10^{-3}$ g (g of solution)$^{-1}$ quenched from the unimer region to the different temperatures, 12 °C (▽) and 21 °C (◆).

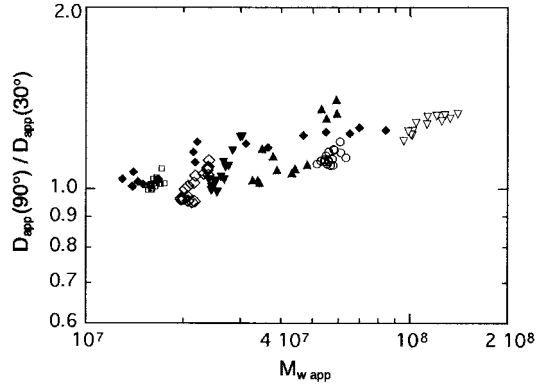

Figure 12. Plots of $D_{app}(90°)/D_{app}(30°)$ vs $M_{w,app}$. Symbols are the same as those in Figure 11.

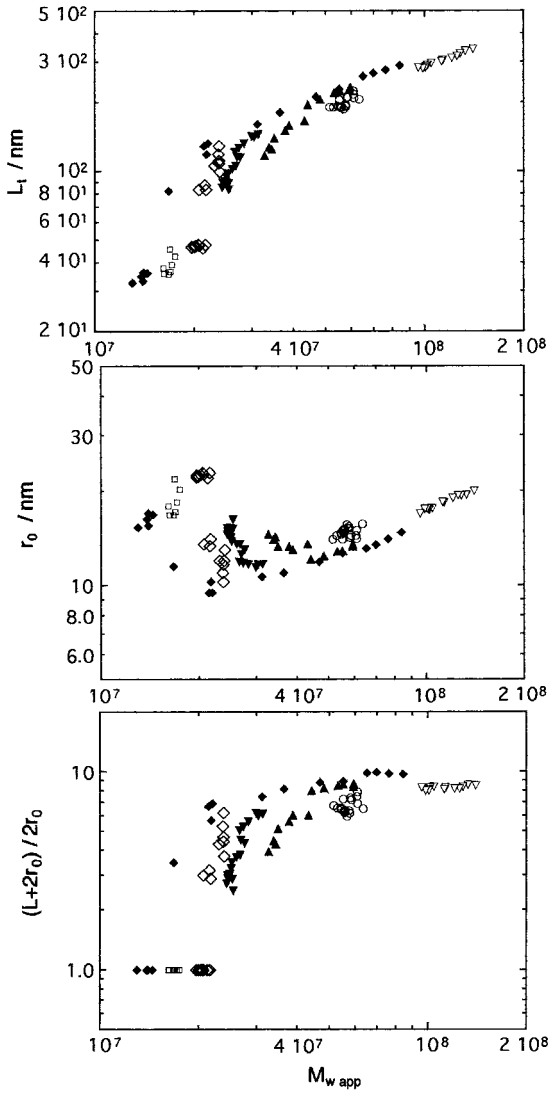

Figure 13. Plots of L_t, r_0, and $(L + 2r_0)/2r_0$ vs $M_{w,app}$. Symbols are the same as those in Figure 11.

celles under almost no change of unimer concentration. The large cylindrical micelles are formed in the first fast process and are very stable, like in a metastable state, once they have been formed, since the following slow process is so slow. Following this picture of micellization, the formation of the large micelles, being larger than the equilibrium micelle, implies that the growth rate of micelles is sufficiently large compared with the rate of generation of new micelles. The growth rate is larger than the rate that would be expected in the case where the micellization goes on with monotonical change of micelle size, showing no maximum and maintaining the spherical shape. The experimental finding that the large micelles are more easily formed in more dilute solutions can consistently be explained by the less frequent birth of new micelles that is generally expected at the lower concentration.[23] The large growth rate and the small birth rate of micelles, which lead to the formation of large cylindrical micelles in the micellization from the unimer state, probably originate from the bilayer structure of micelles, i.e., the vesicle structure. A block copolymer chain in the outer layer goes to the inner layer to make the bilayer structure less easily than a unimer chain in the pool of solution enters the outer layer of a micelle, because the free energy barrier for a block copolymer chain to move from the outer to the inner layer must be high due to immiscibility between constitutional block chains. Therefore, the growth rate of the bilayer structure of the spherical micelle must be low, compared with that in the monolayer structure, since many of copolymer chains have to enter the inner layer. This is also the case in the birth process of bilayer micelles, resulting in the slow generation of new micelles. Consequently, in the growth process of a micelle, the number of copolymer chains in the outer layer increases faster than that of the inner layer, bringing about the elongation of micelle shape to decrease the curvature. This structural change can make the increase of association number more easily, i.e., make the micellar growth in the first process faster than that in the case of a spherical bilayer micelle.

As to the micellar rearrangements in condition 1, the increase of micelle size at 12 °C after cooling from 36 °C is probably brought about by the work of the same mechanism as that above-described for the micellization but does not simply correspond to the increase of $M_{w,app}$ in the first fast process of micellization from the unimer state in condition 2. An essential difference between them is seen in the time scale. That is, the micellar rearrangements in condition 1 go on very slowly, while the fast process of micellization finishes within 100 s. The difference should be attributed to that in the initial state of solution between the two conditions. In condition 1, most of the unimers have already been consumed to form micelles when the micelle growth starts at 12 °C, which may cause slowing of the rate of further micelle growth because of a lack of free unimers in the solution. On the other hand, the micellization in condition 2 starts under the presence of a large amount of free unimers. Micellar rearrangements may delicately be controlled by the state of micellar solution, such as unimer concentration and association number with its distribution, which can lead to complex process dependency of micelle size and structure.

To demonstrate the reality of the above explanation, we further need a more quantitative theoretical description for time evolution of the micelle morphology, which we are currently investigating, as well as more direct observations of the morphology.

Conclusions

The present experimental results clearly show nonmonotonical changes of the micelle size during both processes of micellar relaxation and micellization from the unimer state, demonstrating that large cylindrical micelles can be kinetically formed. Furthermore, we have successfully observed, for the first time to our knowledge, that the structural changes of micelles can take place completely kinetically in the course of micelle formation. The nonmonotonical micellization from the unimer state proceeds through the fast process followed by the slow process. In the first fast process, micelles are born and grow by consuming large amounts of excess free unimers in the solution. The larger cylindrical micelles are formed during the fast process and are so stable as to be regarded as metastable micelles because the second slow process of approaching the equilibrium is slow enough, which arises from the fact that the reorganization of micelles can be made only by the insertion and expulsion under almost no excess free unimers in the pool of solution. The bilayer structure of micelles (vesicles) formed in the present system gives

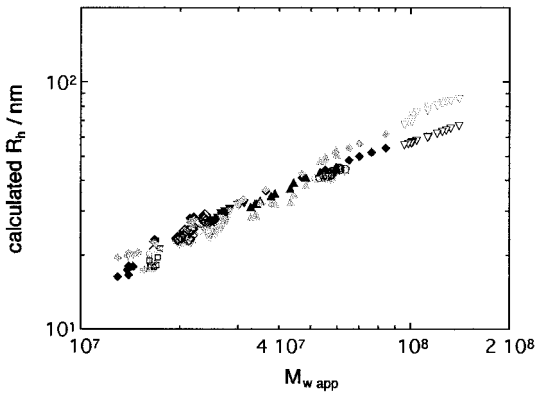

Figure 14. Comparison of the values of R_h (solid plots) calculated by eq A-3 and the experimental values of $R_{h,app}$ (draft plots). Symbols are the same as those in Figure 11.

a reasonable account for the less frequent birth and the rapid growth of micelles, which lead to the nonmonotonical change of the micelle size and the formation of cylindrical micelles. Namely, the rate of copolymer diffusion from the outer layer to the inner layer is expected to be smaller than that from the pool of solution to the outer layer, which brings about the slow new-micelle generation and the elongation of the micelle shape for the rapid growth, with the increase of association number in the outer layer dominating that in the inner layer.

Appendix: A Quantitative Analysis of Micelle Shape by the Model of a Rigid Hemispherical Hollow Cylinder

A rigid hollow cylinder with a pair of hollow hemispheres at its ends is demonstrated to fairly well describe the shape of the present micelles in our previous study.[16] Adopting this model, the outside radius r_0 of the core and the length of cylinder L excluding the hemisphere parts can be estimated from the experimental values of $M_{w,app}$ and $R_{g,app}$. Namely, r_0 and L can be calculated from the following expressions for the molar mass $M_{w,core}$ and the radius of gyration $R_{g,core}$ of the core.

$$M_{w,core} = N_A\rho\left[\frac{4}{3}\pi(r_0^3 - r_1^3) + \pi L(r_0^2 - r_1^2)\right] \quad \text{(A-1)}$$

$$R_{g,core}^2 = \frac{\frac{4}{5}(r_0^5 - r_1^5) + L(r_0^4 - r_1^4) + \frac{L^2}{3}(r_0^3 - r_1^3) + \frac{L^3}{12}(r_0^2 - r_1^2)}{\frac{4}{3}(r_0^3 - r_1^3) + L(r_0^2 - r_1^2)} \quad \text{(A-2)}$$

where r_1 is the inside radius of the core. Here, $M_{w,core}$ is given by multiplying $M_{w,app}$ by the composition of the core, $R_{g,core}$ is put to be equal to $R_{g,app}$, and the thickness $r_0 - r_1$ of the core is estimated to be $r_0 - r_1 = 4.2$ nm,[16] independent of r_0 and L. The data plotted in Figure 13 were thus obtained.

The obtained values of r_0 and L consistently reproduce the experimentally observed $R_{h,app}$. That is, as illustrated in Figure 14, the hydrodynamic radius R_h calculated from the r_0 and L values obtained from $M_{w,app}$ and $R_{g,app}$ reasonably agree with the experimental $R_{h,app}$ as long as $M_{w,app}$ is not so large. The flexibility cannot be neglected at large $M_{w,app}$'s. Here, R_h is calculated by using Norisuye's formula[37] for a rigid hemispherical cylinder.

$$\frac{L_t/2}{R_h} = \ln\frac{2L_t - 2R + \{4L_t^2 - 4L_t(2R) + 2(2R)^2\}^{1/2}}{2R} + \frac{L_t + 2^{1/2}(2R) - \{4L_t^2 - 4L_t(2R) + 2(2R)^2\}^{1/2}}{L_t} + \{(2R)/2L_t\} \times \ln\frac{(2^{1/2} - 1)^2[2R + \{4L_t^2 - 4L_t(2R) + 2(2R)^2\}^{1/2}]}{2L_t - 2R + \{4L_t^2 - 4L_t(2R) + 2(2R)^2\}^{1/2}} \quad \text{(A-3)}$$

where R and L_t are the radius of the cylinder and the total contour length ($L + 2R$), including the corona, respectively, and the thickness of the outside corona is put as $R - r_0 = 1.1$ nm.[16]

References and Notes

(1) Tuzar, Z.; Kratochvíl, P. In *Surface and Colloid Science*; Matijević, E., Ed.; Plenum Press: New York, 1993; Vol. 15, pp 1−83.
(2) Mortensen, K.; Pedersen, J. S. *Macromolecules* **1993**, *26*, 805−812.
(3) Mortensen, K.; Brown, W. *Macromolecules* **1993**, *26*, 4128−4135.
(4) Schillén, K.; Brown, W.; Johnsen, R. M. *Macromolecules* **1994**, *27*, 4825−4832.
(5) Mortensen, K.; Brown, W.; Jørgensen, E. *Macromolecules* **1994**, *27*, 5654−5666.
(6) Wennerström, H.; Lindman, B. *Phys. Rep.* **1979**, *52*, 1−86.
(7) Tsunashima, Y. *Macromolecules* **1990**, *23*, 2963−2969.
(8) Price, C.; Chan, E. K. M.; Hudd, A. L.; Stubbersfield, R. B. *Polym. Commun.* **1986**, *27*, 196−198.
(9) Stejskal, J.; Hlavatá, D.; Sikora, A.; Koňák, Č.; Pleštil, J.; Kratochvíl, P. *Polymer* **1992**, *33*, 3675−3685.
(10) Stejskal, J.; Koňák, Č.; Helmstedt, M.; Kratochvíl, P. *Collect. Czech. Chem. Commun.* **1993**, *58*, 2282−2289.
(11) Hlavatá, D.; Stejskal, J.; Pleštil, J.; Koňák, Č.; Kratochvíl, P.; Helmstedt, M.; Mio, H.; Laggner, P. *Polymer* **1996**, *37*, 799−805.
(12) Yu, K.; Zhang, L.; Eisenberg, A. *Langmuir* **1996**, *12*, 5980−5984.
(13) Zhang, L.; Shen, H.; Eisenberg, A. *Macromolecules* **1997**, *30*, 1001−1011.
(14) Tao, J.; Stewart, S.; Liu, G.; Yang, M. *Macromolecules* **1997**, *30*, 2738−2745.
(15) Ding, J.; Liu, G.; Yang, M. *Polymer* **1997**, *38*, 5497−5502.
(16) Iyama, K.; Nose, T. *Polymer* **1998**, *39*, 651−658.
(17) Ehl, P. J.; Loucheux, C.; Reiss, C.; Benoit, H. *Makromol. Chem.* **1964**, *75*, 35−51.
(18) Moreels, E.; De Ceuninck, W.; Finsy, R. *J. Chem. Phys.* **1987**, *86*, 618−623.
(19) Finnigan, J. A.; Jacobs, D. J. *Chem. Phys. Lett.* **1970**, *6*, 141−143.
(20) Honda, C.; Abe, Y.; Nose, T. *Macromolecules* **1996**, *29*, 6778−6785.
(21) Michels, B.; Waton, G.; Zana, R. *Langmuir* **1997**, *13*, 3111−3118.
(22) Goldmints, I.; Holzwarth, J. F.; Smith, K. A.; Hatton, T. A. *Langmuir* **1997**, *13*, 6130−6134.
(23) Honda, C.; Hasegawa, Y.; Hirunuma, R.; Nose, T. *Macromolecules* **1994**, *27*, 7660−7668.
(24) Aniansson, E. A. G. In *Aggregation Processes in Solution*; Wyn-Jones, E., Gormally, J., Eds.; Elsevier: Amsterdam, 1983; pp 70−99.
(25) Aniansson, E. A. G.; Wall, S. N. *J. Phys. Chem.* **1974**, *78*, 1024−1030.
(26) Aniansson, E. A. G.; Wall, S. N.; Almgren, M.; Hoffmann, H.; Kielmann, I.; Ulbricht, W.; Zana, R.; Lamg, J.; Tondre, C. *J. Phys. Chem.* **1976**, *80*, 905−922.
(27) Halperin, A. *Europhys. Lett.* **1989**, *8*, 351−356.
(28) Halperin, A.; Alexander, S. *Macromolecules* **1989**, *22*, 2403−2412.
(29) Halperin, A.; Tirrell, M.; Lodge, T. P. *Adv. Polym. Sci.* **1992**, *100*, 31−71.

(30) Bednář, B.; Edwards, K.; Almgren, M.; Tormod, S.; Tuzar, Z. *Makromol. Chem. Rapid Commun.* **1988**, *9*, 785−790.
(31) Hecht, E.; Hoffmann, H. *Colloid Surf.* **1995**, *96*, 181−197.
(32) Wang, Y.; Kausch, C. M.; Chun, M.; Quirk, R. P.; Mattice, W. L. *Macromolecules* **1995**, *28*, 904−911.
(33) Smith, C. K.; Liu, G. *Macromolecules* **1996**, *29*, 2060−2067.
(34) Wang, Y.; Mattice, W. L.; Napper, D. *Langmuir* **1993**, *9*, 66−70.
(35) Haliloğlu, T.; Mattice, W. L. *Chem. Eng. Sci.* **1994**, *49*, 2851−2857.
(36) Haliloğlu, T.; Bahar, I.; Erman, B.; Mattice, W. L. *Macromolecules* **1996**, *29*, 4764−4771.
(37) Norisuye, T.; Motowoka, M.; Fujita, H. *Macromolecules* **1979**, *12*, 320−323.

MA980501T